VERSITA

OPTO-ELECTRONICS REVIEW **14**(1), 54–58 DOI: 10.2478/s11772-006-0008-y

Uncooled thermo-mechanical detector array with optical readout

H. TORUN and H. UREY*

Koç University, Sariyer, 34450 Istanbul, Turkey

This paper reports a novel uncooled infrared FPA whose performance is comparable to the cooled FPA's in terms of noise parameters. FPA consists of bimaterial microcantilever structures that are designed to convert IR radiation energy into mechanical energy. Induced deflection by mechanical energy is detected by means of optical methods that measure sub nanometer thermally induced deflections. Analytical solutions are developed for calculating the figure of merits for the FPA. FEM simulations and the analytical solution agree well. Calculations show that for an FPA, NETD of < 5 mK is achievable in the 8–12 μm band. The design and optimization for the detectors are presented. The mechanical structure of pixels is designed such that it can be possible to form large array size FPA's. Microfabrication of the devices to improve the performance further, employs low cost standard MEMS processes.

Keywords: infrared detectors, optical sensor, bimaterial cantilever.

1. Introduction

Although the cooled infrared detectors offer good performance, they have some important drawbacks such as the need for the cryogenic coolers, having high cost, and responding to specific spectral bands. Research on uncooled thermal detectors has been going on to offer a technology to solve these problems so, that it will be feasible to use cameras for night vision applications. The microbolometer technology is the most mature one among other uncooled thermal detector technologies like pyroelectric detectors or thermopiles in the sense that they offer both better noise performance and resolution. Microbolometers are now realized in large size focal plane arrays [1,2]. The ultimate performance level expected from uncooled thermal detector technologies is given by Kruse in Ref. 3. The noise analysis for these detectors shows that the performance of such detectors is limited mostly by the readout noise. Moreover, it is necessary to pass electrical current through the pixels in order to sense the induced temperature difference. The electrically conductive materials needed to provide paths for the electrical signal increase the thermal conductance of the detector, which is another important limitation for the microbolometers. Recently, a new kind of thermal detector technology based on microcantilevers is introduced. Both electrostatic [4] and optical readout [5] methods are offered with the microcantilever type detectors. It is demonstrated that microcantilever sensors offer high sensitivity like atomic force microscopes and biological detectors. Furthermore, with the help of the optical readout method, the thermo-mechanical detector can be decoupled from the readout, allowing to optimize each separately. Since such a detector has no electrical connections to the IR detector, it is possible to decrease the thermal conductance. Our design offers not only higher performance with low NETD values but also an integrated optical readout scheme in a scalable architecture.

2. IR absorber design

The thermal camera FPA is based on pixels composed of membranes with bimaterial legs. The infrared radiation is absorbed in the absorption pad, which is a thin layer of silicon nitride (SiN_x), which is a good absorber in 8–12 μm infrared band. The real and imaginary parts of refractive index of silicon-rich nitride film with respect to the radiation wavelength are known [6]. As shown in Fig. 1, the absorption calculations based on this data shows that the maximum absorption that can be achieved in 2–16 μm infrared band is slightly larger than 50% for a layer thickness of 0.5 μm. The assumption for the calculations is that the active layer is kept in the vacuum and single pass of the radiation through the active layer is allowed. The absorption can be increased by increasing the layer thickness since the absorptance depends on the active layer thickness by $1 - \exp(-\alpha d)$ where α is the absorption constant and d is the thickness of the layer. On the other hand, further increase in the active layer would increase the thermal mass of the detector, which would increase the time constant and reduce the frame rates for the detector array.

One common solution to increase the absorptance without making the detector slower is to implement a resonant cavity between the active layer and the substrate. The absorption of IR radiation can be enhanced due to the interaction between the optical signal passing through the active

*e-mail: hurey@ku.edu.tr

The paper presented there appears in *Infrared Photoelectronics*, edited by Antoni Rogalski, Eustace L. Dereniak, Fiodor F. Sizov, Proc. SPIE Vol. 5957, 59570O (2005).

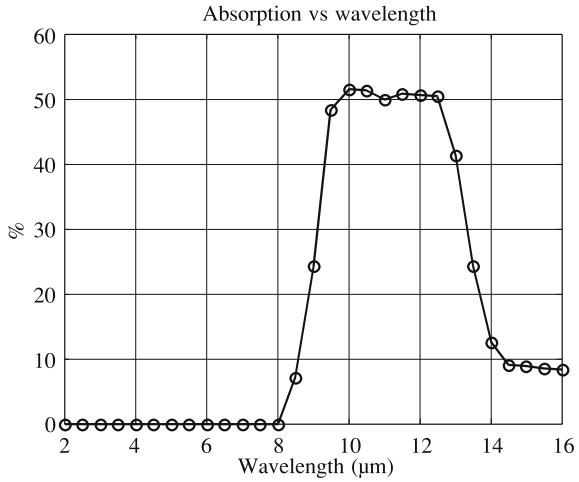

Fig. 1. Absorption of IR radiation by thin nitride layer based on single pass of radiation based on the data given in Ref. 6.

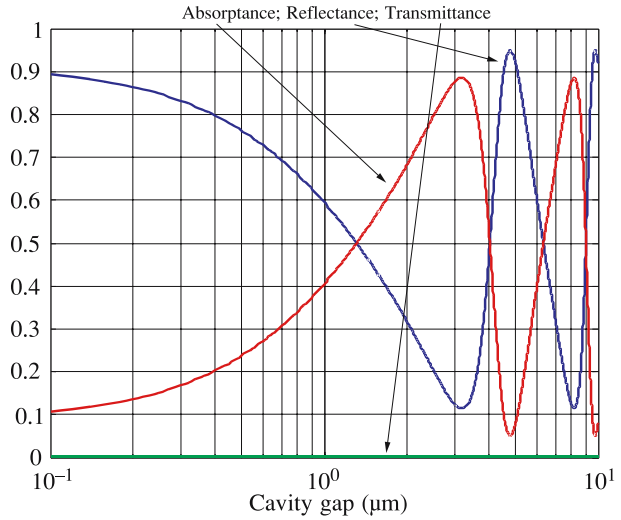

Fig. 3. Absorption at 10-μm wavelength as a function of resonant cavity gap.

layer and the one reflected from the substrate. The requirement for the presence of optical signals in both directions is that the thickness of the active layer is smaller than the penetration depth of the radiation at a specific wavelength. For that condition, the absorption can be increased significantly at specific wavelengths as a result of this fact if the substrate is coated with a reflector to provide the optical signal in propagating in the reverse direction. The IR reflectors shown in cross sectional schematics of the detector pixels in Fig. 2 serve as the reflector to form the resonant cavity. By changing the gap between the absorption layer and the reflector of the cavity, the wavelength at which the absorption is maximized can be engineered. For this design, the resonant cavity is designed such that the absorption at the wavelength of 10 μm is maximized since that is the point at which a blackbody at room temperature (300 K) has its spectral exitance peak. The plot given in Fig. 3 shows the dependence of absorptance to the radiation wavelength. Theoretically, it is expected to have the peak point at a gap of quarter of the wavelength. Since the metal grating layer is not a perfect reflector, the absorptance peak point shifts as seen from Fig. 3.

The absorption is maximum when the gap of the resonant cavity is around 2.5 μm, independently of the active layer thickness. Therefore it is possible to further optimize the IR absorber to maximize the absorption at the wavelength of 10 μm, centre of the LWIR band, by varying the thickness of the nitride layer. Calculations show that the peak absorptance level is achieved when the active layer is of 770-nm thick. The analytical model predicts absorption, transmission and reflectance for n layers considering the penetration depth into account, which is given as

$$d_{penetration} = \frac{\lambda}{4\pi k}, \tag{1}$$

where k is the imaginary part of the refractive index of the material and λ is the wavelength of the radiation. From Eq. (1), k is around unity for the band of 8–12 μm, which makes the penetration depth of approximately 0.8 μm. This fact can be also seen from Fig. 4 where absorptance is plotted as a function of active layer thickness. When the active layer is thicker than the penetration depth, absorptance degrades since the resonant cavity is not functional anymore.

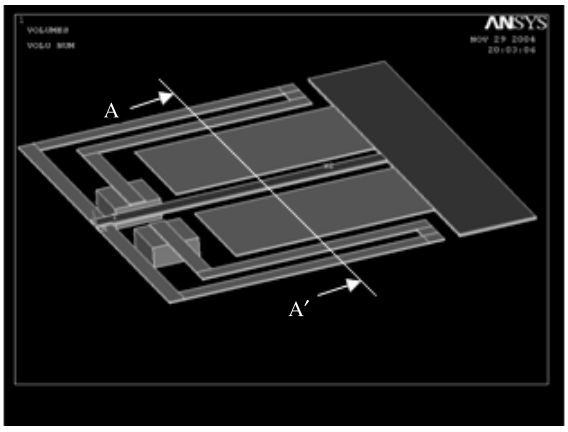

(a)

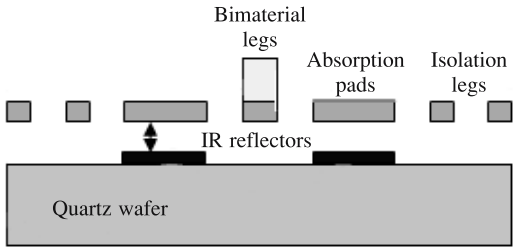

(b)

Fig. 2. One pixel of FPA (a) and cross section of the detector pixels (b).

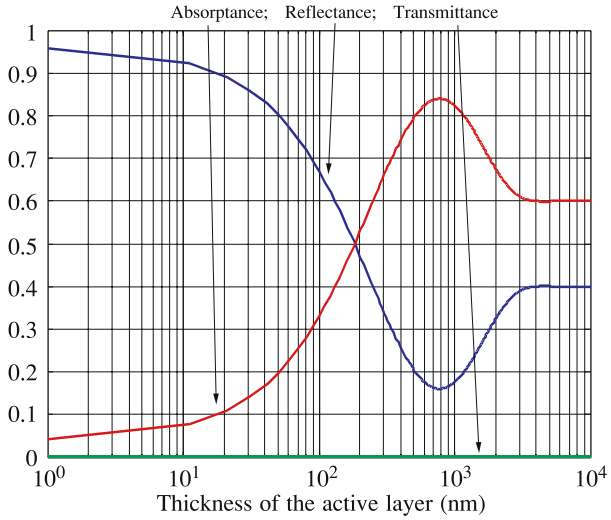

Fig. 4. Variation of absorptance using 2.5-μm resonant cavity as a function of nitride layer thickness.

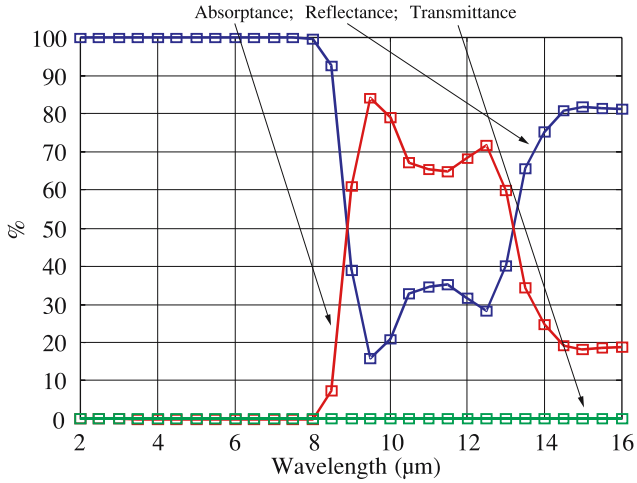

Fig. 5. Spectral response of 0.5-μm thick SiN_x layer in the 2–16-μm wavelength range including a resonant cavity with 2.5-μm gap.

From this analysis, the absorption characteristics of the design are optimized and the spectral response of the detector in the 2–16-μm band is shown in Fig. 5.

3. Bending of microcantilevers

The temperature induced on the detectors as a result of radiation absorption is converted into mechanical deflection by the help of the bimaterial legs that support the membranes. Since the deflection is to be sensed by optical means, the deflection per Kelvin temperature induced on the detectors should be maximized. The amount of deflection depends on the material properties as well as on the thicknesses and lengths of the cantilever legs and for one sided clamped n layer thin films the deflection is given by the following equations [7]

$$\begin{bmatrix} 1 & 1 & 1 & \cdots & 1 & 0 \\ \frac{h_1}{2} & h_1+\frac{h_2}{2} & h_1+h_2+\frac{h_3}{2} & 0\ \cdots & h_1+h_2+\ldots+\frac{h_m}{2} & \sum_{i=1}^{m}\frac{E_i b h_i^3}{12} \\ \frac{1}{E_1 b h_1} & \frac{-1}{E_2 b h_2} & 0 & 0\ \cdots & 0 & \frac{h_1+h_2}{2} \\ 0 & \frac{1}{E_2 b h_2} & \frac{-1}{E_3 b h_3} & \cdots & 0 & \frac{h_2+h_3}{2} \\ & & & \vdots & \vdots & \\ 0 & 0 & \cdots & 0\ \frac{1}{E_{m-1} b h_{m-1}} & \frac{1}{E_m b h_m} & \frac{h_{m-1}+h_m}{2} \end{bmatrix} \begin{bmatrix} N_1 \\ N_2 \\ \vdots \\ N_m \\ 1/\rho \end{bmatrix} = \begin{bmatrix} 0 \\ 0 \\ (\alpha_2-\alpha_1)\Delta T \\ (\alpha_3-\alpha_2)\Delta T \\ \vdots \\ (\alpha_m-\alpha_{m-1})\Delta T \end{bmatrix}, \quad (2)$$

$$\delta = \frac{1}{2\rho} L^2 \Delta T, \quad (3)$$

where h_i, E_i, N_i, α_i, b, L, ΔT, and ρ are the thickness, Young's modulus, effective normal force, CTE, width, length, temperature difference and radius of curvature for the layer i and δ is the deflection from the equilibrium point. The expected deflection along the bimaterial leg can be predicted by the given analytical model. Analytical calculations are compared with the finite element simulation by ANSYS™ for a bimaterial layer made of 500 nm Al and 500 nm nitride layers. FEM gives a deflection of 45.38 nm/K as seen from Fig. 6(a) which is in very good agreement with the analytical calculations that predict a deflection of 43.89 nm per Kelvin introduced on the pixels.

The contour plots given in Fig. 6(b) shows the expected deflections for 1 K temperature difference on the pixels as a function of Al and SiN_x thicknesses. It can be clearly seen that as the layers become thinner, the deflection increases, so does the sensitivity. Moreover, the heat capacity of the detector decreases since thermal mass decreases. That makes fast detection possible. On the other hand, as the layers get thinner, uniformity of the pixels degrades and stress of the layers cannot be controlled well due to microfabrication variations. One other drawback of having thinner layers is in terms of noise. Thermo-mechanical noise, which is discussed in the following part, would become dominant in that case. Considering these facts, optimum values for the layer thicknesses can be found.

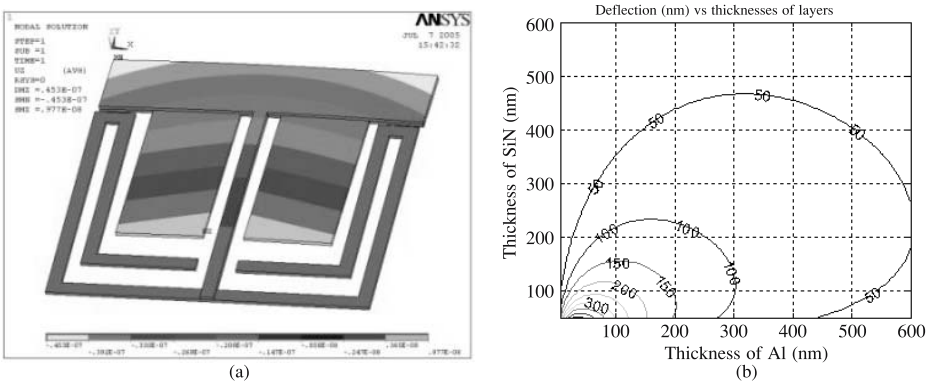

Fig. 6. FEM result of thermomechanical deflection for the selected pixel geometry (a) and analytical calculation for the deflection as a function of layer thicknesses per 1 K temperature difference (b).

4. Noise and NETD analysis

Thermomechanical noise is the fundamental noise source to the nature of the mechanical structures such as microcantilever based thermal detectors. The driving force of this noise source is the thermal energy which specifies the average amount of thermally induced energy that is available per mode of the moving mechanical structure. For any mechanical structure, there is a continuous energy exchange between the mechanically stored energy and the thermal energy present in the environment since the ideal decoupling between the structure and its environment is not possible.

Microcantilever thermal detectors can be considered as mechanical resonators. The described energy exchange causes some mechanical fluctuations in the vibrating microcantilever. For off-resonance operation, the mechanical fluctuations can be combined with the noise equivalent temperature difference (*NETD*) expressions derived for the performance analysis of thermal detectors [3]. *NETD* gives a metric measure of how sensitive the detector is in a sense that it is the minimum resolvable temperature difference of a blackbody source placed in front of a thermal detector. Therefore *NETD* as a result of thermomechanical noise is [8]

$$NETD_{TM} = \frac{8 f_{no}^2 G \sqrt{k_B T_D \Delta f}}{\eta \tau_0 \beta A (dP/dT)_{\lambda 1-\lambda 2} R \sqrt{k \omega_0 Q}}, \qquad (4)$$

where f_{no} is the *f*-number of the IR optics, G is the thermal conductance, k_B is the Boltzmann's constant, T_D is the temperature, and Δf is the bandwidth of the detector; k, Q, and ω_0 are the spring constant, quality factor and resonant frequency of the mechanical structure, respectively. η is the emissivity of the detector, τ_0 is the transmittance of the medium in which IR radiation is propagating and (dP/dT) shows the change in power per unit area radiated by a blackbody measured within the spectral windows λ_1 to λ_2 and R is the mechanical responsivity of the detector to the temperature induced on it.

Thermal fluctuation (TF) noise is the fundamental noise source for all types of thermal detectors since it causes fluctuations on the temperature of a detector as a result of continuous heat exchange between the detector and its environment. The fluctuations on the temperature can be minimized if the detector is thermally isolated from its environment. At best, the heat exchange is through radiation. Since this is a special condition, the noise associated to it is examined separately. Sticking to the definitions given before, the temperature fluctuation should be related to the noise magnitude of mechanical displacement in order to calculate the noise equivalent temperature difference value associated with temperature fluctuation noise as [8]

$$NETD_{TF} = \frac{8 f_{no}^2 T_D \sqrt{k_B G \Delta f}}{\eta \tau_0 \beta A (dP/dT)_{\lambda 1-\lambda 2}}. \qquad (5)$$

The special condition mentioned for the thermal fluctuation noise is background fluctuation noise, which gives the fundamental limit for any kind of device that is used to detect infrared radiation. As shown in the thermal fluctuation case, the noise is directly proportional to the thermal conductance of the detector. Thermal conductance for any type of structure cannot be minimized further than the value for which the heat exchange between the detector and the environment is through radiation. For this case, if the thermal conductance, which is purely due to radiation, is put into the *NETD* expression given in Ref. 9, the background fluctuation noise is given as [8]

$$NETD_{BF} = \frac{16 f_{no}^2 T_D \sqrt{k_B \sigma \Delta f T_D^5}}{\eta \tau_0 \sqrt{\beta A} (dP/dT)_{\lambda 1-\lambda 2}}, \qquad (6)$$

where σ is the Stefan-Boltzmann's constant. The noise components for the design prototype are plotted as a function of thermal conductance of pixel in Fig. 7. It is crucial to optimize the pixels such that the thermal conductance would be minimized for better performance levels. In terms of *NETD*, going below 10 mK is challenging for thermal detectors. It is calculated that $NETD_{BF}$ = 1.3 mK, $NETD_{TF}$ = 7.1 mK, and $NETD_{BF}$ = 2.1 mK which makes total *NETD* 7.5 mK with the current thermal isolation level for the fabricated thermal detector pixels. Further improvements in thermal isolation can be possible by optimizing the thermal isolation legs such that making the legs narrower by decreasing the minimum linewidth for the microfabrication.

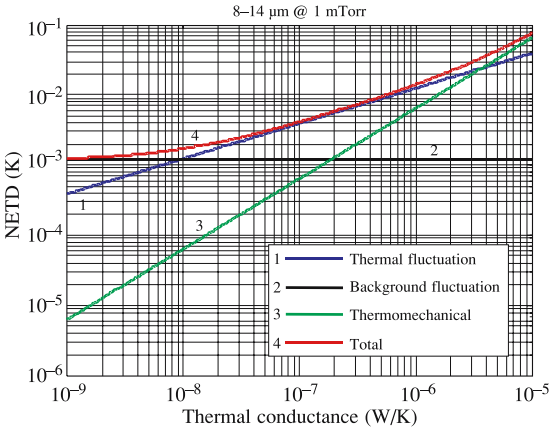

Fig. 7. NETD as a function of thermal conductance *G*.

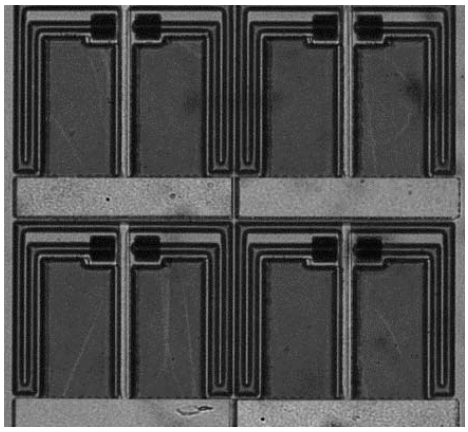

Fig. 8. Fabricated thermal detector pixels.

Moreover, with the optimization of IR absorber and bimaterial legs given previously, it is possible to have an *NETD* value less than 5 mK.

5. Fabrication

Surface micromachining techniques are used to fabricate the thermal detector pixels. The whole process is a four mask one. The process is started with a quartz wafer in order to provide an optically transparent substrate. The top view of a portion of the fabricated detector array is given in Fig. 8. First, an aluminium layer is deposited by evaporation on top of quartz wafer and then patterned by lift-off technique in order to provide the IR reflector. Cr layer is used as an adhesion layer due to the poor adhesion between Al and quartz. Then, a sacrificial layer of Cr is deposited using DC sputterer followed by anchors definition shown. Low stress silicon nitride layer is deposited using PECVD. The nitride layer is deposited at low temperature since there are metal layers under the dielectric layer. Stress of the deposited film is controlled by changing the ratio of $He:N_2$ gasses during deposition. The nitride layer provides structural layer for the free-standing structure as well as it provides thermal isolation legs due to its low thermal conductance, infrared absorption pads for 8–14 μm band. On top of the dielectric layer, Al layer is deposited by DC sputterer in order to form the bimaterial legs. CTE of Al (~24 μm/mK) is much larger than that of SiN_x (~0.8 μm/mK) so that significant deflection can be observed during operation. The nitride layer is patterned to create the absorption pad and isolation legs using RIE. Finally, Cr sacrificial layer is etched using wet etching techniques to release the devices. Pixels are designed such that it would be easy to form large size arrays as shown in Fig. 8.

6. Conclusions

We designed and fabricated a novel uncooled thermal detector based on microcantilevers. The deflection of the microcantilevers is measured by means of optical methods that free the electrical ports. By the described optimizations it is possible to achieve an *NETD* value of 5 mK in the 8–12 μm IR band. The mechanical structures of the pixels are scalable and it is possible to integrate the pixel level optical readout to the structure. As a result of this, the architecture is possible to form large size focal plane arrays. The design prototype was fabricated on the top of a quartz wafer using surface micromachining techniques using standard materials that are commonly used in IC industry. Microfabrication of the design employs a low cost and four-mask process. Further improvements in terms of noise performance are possible by optimizing the microfabrication levels and reducing minimum line width. The IR detector arrays are currently being tested in our laboratories.

References

1. S. Eminoglu, M.Y. Tanrikulu, and T. Akin, "Low-cost 64×64 uncooled infrared detector arrays in standard CMOS", *Proc. 12th Int. Conf. on Solid-State Sensors and Actuators* (*TRANSDUCERS'03*) **1**, 316–319 (2003).
2. D.F. Murphy, M. Ray, R. Wyles, J.F. Asbrock, N.A. Lum, A. Kennedy, J. Wyles, C. Hewitt, G.E. Graham, T. Horikiri, J.S. Anderson, D. Bradley, R. Chin, and T. Kostrzewa, "High sensitivity (25 μm pitch) microbolometer FPAs", *Proc. SPIE* **4454**, 147–159 (2001).
3. P.W. Kruse, "Principle of uncooled infrared focal plane arrays", *Semiconductors and Semimetals* **47**, 17–44 (1997).
4. S.R. Hunter, R.A. Amantea, L.A. Godman, D.B. Kharas, S. Gershtein, J.R. Matey, S.N. Perna, Y. Yu, N. Maley, and L.K. White, "High sensitivity uncooled microcantilever infrared imaging arrays", *Proc. SPIE* **5074**, 469–480 (2003).
5. Y. Zhao, M. Mao, R. Horowitz, A. Majumdar, J. Varesi, P. Norton, and J. Kitching, "Optomechanical uncooled infrared imaging system: design, microfabrication, and performance", *J. Microelectromech. Syst.* **11**, 136–146 (2002).
6. Y. Zhao, "Optomechanical uncooled infrared imaging system", *PhD Dissertation*, University of California, Berkeley, Fall 2002.
7. H. Torun, H. Urey, and F. DeWitt, "Thermal deformation and athermalization of multil layered MEMS structures", submitted (2005).
8. P.G. Datskos, N.V. Lavrik, and S. Rajic, "Performance of uncooled microcantilever thermal detectors", *Review of Scientific Instruments* **75**, 1134–1148 (2004).

